Ultra-robust high-field magnetization plateau and supersolidity in bond-frustrated MnCr2S4

Vladimir Tsurkan, Sergei Zherlitsyn, Lilian Prodan, Viorel Felea, Pham Thanh Cong, Yurii Skourski, Zhe Wang, Joachim Deisenhofer, Hans-Albrecht Krug von Nidda, Joahim Wosnitza, Alois Loidl

Angaben zur Veröffentlichung / Publication details:

Tsurkan, Vladimir, Sergei Zherlitsyn, Lilian Prodan, Viorel Felea, Pham Thanh Cong, Yurii Skourski, Zhe Wang, et al. 2017. "Ultra-robust high-field magnetization plateau and supersolidity in bond-frustrated MnCr2S4." *Science Advances* 3 (3): e1601982. https://doi.org/10.1126/sciadv.1601982.

CONDENSED MATTER PHYSICS

Ultra-robust high-field magnetization plateau and supersolidity in bond-frustrated $MnCr_2S_4$

Vladimir Tsurkan,[1,2]* Sergei Zherlitsyn,[3] Lilian Prodan,[2] Viorel Felea,[2] Pham Thanh Cong,[3] Yurii Skourski,[3] Zhe Wang,[1] Joachim Deisenhofer,[1] Hans-Albrecht Krug von Nidda,[1] Joahim Wosnitza,[3] Alois Loidl[1]

Frustrated magnets provide a promising avenue for realizing exotic quantum states of matter, such as spin liquids and spin ice or complex spin molecules. Under an external magnetic field, frustrated magnets can exhibit fractional magnetization plateaus related to definite spin patterns stabilized by field-induced lattice distortions. Magnetization and ultrasound experiments in $MnCr_2S_4$ up to 60 T reveal two fascinating features: (i) an extremely robust magnetization plateau with an unusual spin structure and (ii) two intermediate phases, indicating possible realizations of supersolid phases. The magnetization plateau characterizes fully polarized chromium moments, without any contributions from manganese spins. At 40 T, the middle of the plateau, a regime evolves, where sound waves propagate almost without dissipation. The external magnetic field exactly compensates the Cr–Mn exchange field and decouples Mn and Cr sublattices. In analogy to predictions of quantum lattice-gas models, the changes of the spin order of the manganese ions at the phase boundaries of the magnetization plateau are interpreted as transitions to supersolid phases.

INTRODUCTION

Normal spinels with composition AB_2X_4 are ideal candidates for studying magnetic frustration effects: Strong frustration can arise from both the *A* and *B* magnetic cation sublattices. The cations at the *B* site are octahedrally coordinated and form a pyrochlore lattice, one of the strongest contenders of geometric frustration in three dimensions (*1*). The *A*-site cations are tetrahedrally coordinated, constituting a diamond lattice, which is bipartite but susceptible to strong bond frustration effects (*2*). Spin-spiral liquids (*3*) and spin-orbital liquids (*4*) were theoretically predicted and experimentally observed (*5*–*9*) in magnetic *A*-site spinels. In a number of *B*-site chromium oxide spinels, magnetic field–induced transitions to the celebrated half-magnetization plateaus have been detected by high-field studies (*10*–*13*). Theoretically, it has been shown that spin-strain coupling causes the robustness of the half-magnetization plateaus (*12*). Neutron, as well as x-ray, scattering experiments have convincingly proven the strong correlation between spin states and lattice distortion (*13*).

In clear distinction to observations of fractional magnetization in geometrically frustrated chromium oxides, high-field experiments in chromium sulfide and selenide spinels give significantly different results (*14*, *15*). These compounds are dominated by strong bond frustration with competing ferromagnetic and antiferromagnetic (AFM) exchange (*16*). Magnetization and ultrasound experiments in $ZnCr_2S_4$ have revealed a continuous increase of magnetization as a function of an external magnetic field (that is, the absence of any magnetization plateaus) but have established well-defined structural plateaus in the field dependence of the sound velocity (*14*). High-field studies on $CoCr_2O_4$ with magnetic ions also on the *A* sites have revealed an even more complex behavior: a continuous increase of magnetization without any plateau-like regimes but with an unconventional metastable magnetostructural phase (*17*).

[1]Experimental Physics V, Center for Electronic Correlations and Magnetism, Institute of Physics, University of Augsburg, D-86159 Augsburg, Germany. [2]Institute of Applied Physics, Academy of Sciences of Moldova, MD 2028 Chisinau, Republic of Moldova. [3]Hochfeld-Magnetlabor Dresden (HLD–European Magnetic Field Laboratory), Helmholtz-Zentrum Dresden-Rossendorf, D-01314 Dresden, Germany.
*Corresponding author. Email: vladimir.tsurkan@physik.uni-augsburg.de

Concerning the nature of novel high-field states, in recent years, it has been impressively shown that magnetic insulators can open the window to the exciting world of Bose-Einstein condensation of superfluids and supersolids (*18*). In antiferromagnets, magnons can be described as quasi-particles with integer spin, obeying Bose statistics and quantum magnets, and can be effectively regarded as Bose systems. Hence, they can undergo Bose-Einstein condensation and become superfluid or even supersolid. The observation of this exotic phase, a hybrid between a solid and a superfluid, was conjectured long ago (*19*) and has been proposed to exist in liquid ^{4}He (*20*), but the proposal that this phase was supersolid was later discarded (*21*). However, the observation of a supersolid phase in spin systems seems to be a very promising task. Recent experimental studies in ultrahigh magnetic fields suggest that superliquid and supersolid phases could be realized in the geometrically frustrated spinels, with chromium at the *B* site (*11*, *22*–*24*). The identification of supersolid spin states can be based on the analogy of boson and spin systems, as outlined in the pioneering work of Matsuda and Tsuneto (*25*) and Liu and Fisher (*26*). In spin systems, the longitudinal AFM order is an analog of the crystalline order, which, in the quantum lattice-gas model, corresponds to diagonal long-range order (DLRO) (*26*), whereas off-diagonal long-range order (ODLRO), which is characteristic of superfluidity, is the counterpart of transverse (XY) AFM order without longitudinal AFM components. On the basis of symmetry arguments, this analogy should also apply for the paramagnetic and the supersolid phases. The former, with both orders destroyed, corresponds to a liquid, whereas the latter, hosting both orders, is still the missing member in this unified picture of phases corresponding to spin configurations. Note that in this analogy, the ferromagnetic phase is equivalent to the paramagnetic phase.

Here, we present ultrasound and magnetization studies of $MnCr_2S_4$, a spinel with two magnetic sublattices, in magnetic fields up to 60 T at various temperatures. $MnCr_2S_4$ crystallizes in the normal cubic ($Fd3m$) spinel structure, with manganese (Mn^{2+}, $3d^5$ with spin $S = {}^5/_2$) and chromium ions (Cr^{3+}, $3d^3$ with $S = {}^3/_2$) occupying the tetrahedral *A* and octahedral *B* sites, respectively. Extremely weak spin-orbit coupling results from the spin-only behavior of the manganese ions and the half-filled t_{2g} triplet ground state of chromium. Magnetization measurements

reveal the Curie-Weiss law at temperatures above 200 K, with a Curie-Weiss temperature close to 0 K and paramagnetic moments close to the free-ion values (*27*). For lower temperatures, the magnetization evidences two consecutive transitions: (i) at $T_C = 65$ K to a ferrimagnetic state and (ii) at $T_{YK} = 5$ K to a phase with a triangular spin configuration (*27*, *28*). From detailed susceptibility, electron spin resonance, and heat capacity experiments, it has been concluded that in the collinear ferrimagnetic phase, the longitudinal spin component of the manganese spins is antiparallel to the chromium spins, but that the transverse component remains quasi-paramagnetic and disordered (*28*). Extensive theoretical and experimental studies (*29*–*34*) characterized the ground state as a Yafet-Kittel (YK)–type (*35*) canted spin configuration, where the manganese moments at the bipartite *A* site form a triangle with the ferromagnetically ordered *B*-site chromium moments. The order results from strongly competing AFM *AB* (Mn–Cr) and *AA* (Mn–Mn) exchange interactions, in combination with frustration effects. More recent neutron scattering studies (*34*) indicated that the ground state might be even more complex. First high-field magnetization measurements on polycrystalline samples up to 35 T (*36*) identified a further magnetic transition close to 10 T with a significantly increasing slope of the magnetization curve. This phase transition has been interpreted by a model, where the nonequivalent tetrahedral sites bear magnetic moments of different lengths and signs (*36*), alternatively, as a transition to an oblique spin configuration with a canted triangular spin structure with respect to the external field (*37*–*39*) or a specific three-dimensional spin structure (*40*). Our measurements reveal that as a function of external magnetic fields, $MnCr_2S_4$ exhibits a manifold of competing spin states, with the chromium moments always aligned parallel to the external field, but that the manganese spins exhibit different types of transverse and longitudinal order, which, by analogy with bosonic systems, can be described as superliquid and supersolid phases.

RESULTS

YK ground state

Figure 1 documents the magnetic and elastic properties of single-crystalline $MnCr_2S_4$ in zero external magnetic field. At high temperatures, the magnetic susceptibility follows the Curie-Weiss law with an asymptotic Curie-Weiss temperature $\Theta_{CW} \approx 12$ K (Fig. 1A), signaling competing and almost compensated AFM and ferromagnetic exchange interactions typical for strong bond frustration. In the inverse magnetic susceptibility, the ferrimagnetic transition at $T_C = 65$ K is indicated by a clear anomaly, whereas $T_{YK} = 5$ K is only manifested as a weak kink-like feature (inset of Fig. 1A). Below room temperature and on decreasing temperatures, the sound velocity $\Delta v/v$ exhibits pronounced stiffening typical for conventional anharmonic behavior (Fig. 1A). At the ferrimagnetic transition, $\Delta v/v$ shows a step-like stiffening, followed by a further significant increase down to 12 K, where $\Delta v/v$ runs through a maximum and then strongly decreases by almost 1% toward the low-temperature YK transition. This transition shows up as a deep and well-defined minimum in $\Delta v/v$ and a sharp λ-like maximum in the sound attenuation $\Delta\alpha$ (Fig. 1B). The significant changes of the ultrasound velocity at the magnetic transitions and, specifically, at the YK transition indicate the importance of spin-lattice coupling, commonly observed in frustrated magnets.

Note that these anomalies, indicating the triangular spin configuration by slightly canting the manganese spins at $T_{YK} = 5$ K, are much more pronounced compared to those observed at the ferrimagnetic transition at $T_C = 65$ K. This observation will be of prime importance for the interpretation of the high-field results: Obviously, sound velocity and damping are strongly influenced by changes of the manganese spin order, but they are not very sensitive to the onset of collinear chromium order. At the ferrimagnetic transition, the chromium moments are aligned, but the transverse components of the manganese spins remain paramagnetic. The *xy* spin components show order at the YK transition, with concomitant huge effects in sound velocity and damping (Fig. 1B). The Mn–Cr superexchange interaction plays the key role, making the ultrasound sensitive to the spin structure of the Mn sublattice via exchange striction. The sound waves modulate the Mn–Cr distance and the corresponding exchange interaction, resulting in a so-called two-ion magnetoelastic coupling, which is responsible for the observed ultrasound features.

Lotgering's model (*27*) for describing the triangular YK spin configuration of Mn and Cr spins allows us to calculate the exchange

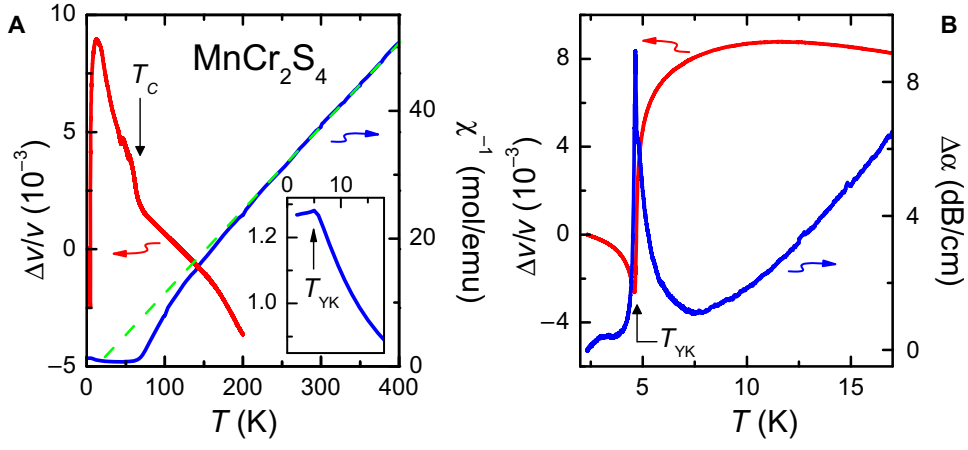

Fig. 1. Temperature dependence of sound velocity and magnetic susceptibility in $MnCr_2S_4$. (**A**) Relative change of the sound velocity $\Delta v/v$ of the longitudinal acoustic mode propagating along the <111> axis in zero magnetic field (left scale). Inverse susceptibility was measured in an external field of 1 T applied along <111> (right scale). The dashed line corresponds to a high-temperature Curie-Weiss law. Inset: Inverse susceptibility versus temperature below 18 K. Vertical arrows mark the ferrimagnetic transition at $T_C = 65$ K and the low-temperature magnetic transition $T_{YK} = 5$ K, establishing a triangular spin configuration. (**B**) Relative change of the sound velocity $\Delta v/v$ (left scale) and sound attenuation $\Delta\alpha$ (right scale) of the same acoustic mode below 20 K. The vertical arrow indicates T_{YK}.

field acting on the manganese spins. In this model, the Mn spins of one sublattice are canted with respect to those of the other Mn sublattice, shifted (¼,¼,¼) along the space diagonal of the cubic unit cell. The resulting moment of the two Mn sublattices is antiparallel to the ferromagnetically aligned Cr spins, as schematically shown in Fig. 2. Below 5 K, the magnetization is temperature-independent, showing a constant slope $d\mathbf{M}/d\mathbf{H}$ = 0.1082 μ_B (Bohr magneton)/T up to about 11 T (Fig. 3). The constant slope results from the continuous increase of the angle between the two Mn sublattices at increasing field. The net magnetization determined from the extrapolation of the linear part of the magnetization curve in the YK phase to zero field equals 1.30 μ_B at 2 K. With these experimentally determined quantities, we calculated the values of the exchange constants J_{AA}/k_B = −1.553 K and J_{AB}/k_B = −1.622 K. These exchange constants are close to the correspondent values J_{AA}/k_B = −1.677 K and J_{AB}/k_B = −1.794 K obtained by Lotgering for polycrystalline $MnCr_2S_4$ (*27*). The estimate of the exchange field $\mathbf{H}_{AA}$ from the four nearest Mn spins acting on each Mn spin of the other sublattice results in a value of $\mu_0\mathbf{H}_{AA} \approx 23$ T. The exchange field acting on each Mn spin from the 12 nearest neighbor Cr spins is estimated as $\mu_0\mathbf{H}_{AB} \approx 43$ T. The canted spin structure could alternatively arise because of Dzyaloshinskii-Moriya (DM) interactions, which break the global U(1) rotational symmetry of the spin degree of freedom. Note that because of the high symmetry of the cubic spinel structure and the specific arrangement of the Mn and Cr sublattices (see Fig. 2), the antisymmetric DM exchange interactions do not play a role because each exchange path has a symmetric counter-path, which compensates any possible DM interactions. Even for the trigonal distortions of the Cr sites, this compensation is preserved. Therefore, any stronger influence of the DM interaction in $MnCr_2S_4$ can be excluded.

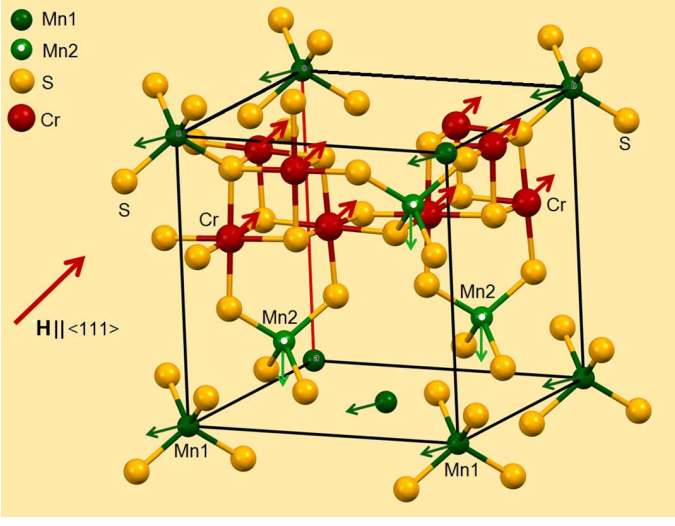

Fig. 2. Illustration of crystallographic and spin structure of $MnCr_2S_4$ at low temperature in the YK phase in external magnetic fields below 10 T. The ferromagnetically aligned Cr spins are always oriented along the external magnetic field. The Mn spins are divided into two sublattices, with canted spin configuration and resulting moment antiparallel to the Cr moments. In the figure, we indicated the directions of the spins of the two Mn sublattices in low field. This angle increases with increasing magnetic field.

High-field plateaus and magnetostructural transitions

Figure 3 shows the magnetization measured in pulsed magnetic fields up to 60 T applied along the <111> direction at temperatures between 1.5 and 28 K. To document the coincidence of critical fields determined by magnetization with those derived via elastic properties, in Fig. 3A, we plotted the magnetization together with the field dependence of the relative change of the sound velocity $\Delta v/v$ at 1.5 K. At the lowest fields, the magnetization $\mathbf{M}(\mathbf{H})$ exhibits an initial domain-derived ferromagnetic-like jump, followed by a linear increase up to 11 T. This is the regime of the triangular YK structure: The chromium moments are aligned in field direction, whereas the manganese spins are antiferromagnetically coupled with finite spin canting, forming a triangular configuration (see Fig. 2). The increase of magnetization with increasing fields is the fingerprint that the angle between the manganese spins opens continuously. At 11 T, $\mathbf{M}(\mathbf{H})$ significantly changes its slope and shows a further continuous increase up to 25 T. In earlier magnetization experiments up to 35 T (*36*), this field regime was described in terms of an oblique (canted), triangular (*37*) or a three-dimensional spin structure (*40*). Between 25 and 50 T, the magnetization exhibits an unusually robust magnetization plateau at a value of 6 μ_B. In this plateau region, the magnetization is determined by fully polarized chromium moments without any net contributions from the manganese spins. Finally, above 50 T, the external field overcomes the AFM Cr–Mn exchange, and the manganese spins flip toward the direction of the external field, resulting in a further increasing magnetization toward the highest applied fields.

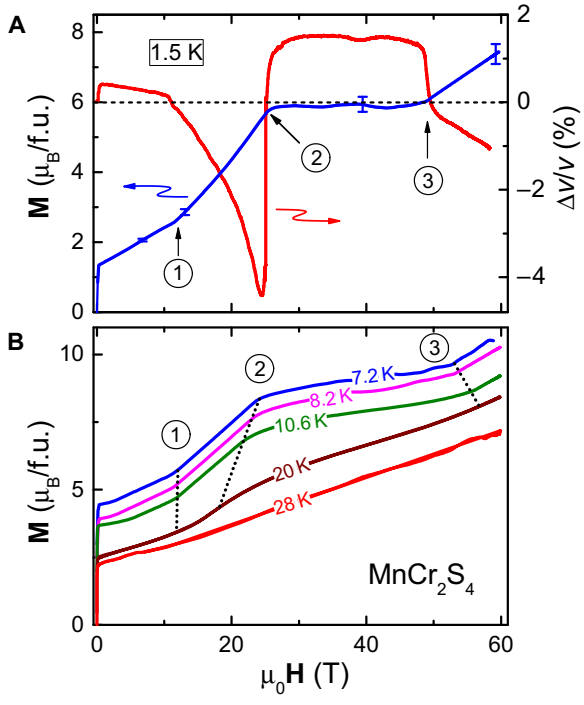

Fig. 3. Field dependence of magnetization and ultrasound velocity in $MnCr_2S_4$ single crystals. (**A**) Magnetization (left scale), in Bohr magneton per f.u. (formula unit), and relative change of the sound velocity $\Delta v/v$ of the longitudinal acoustic mode propagating along the <111> axis (right scale) at 1.5 K as a function of the external magnetic field applied along <111>. Error bars mark uncertainties of calibration, which increase with increasing fields. (**B**) Magnetization for different temperatures between 7.2 and 28 K. For clarity, the curves at T < 28 K are shifted. Anomalies at 11, 25, and 50 T are consecutively numbered, and dotted lines indicate their temperature-dependent shifts.

However, the fully spin-polarized state of chromium and manganese moments, which corresponds to a value of 11 μ_B, is far beyond the field range accessible in the present experiments. In Fig. 3A, the critical fields that indicate subsequent magnetic phase transitions at 11, 25, and 50 T are labeled as anomalies 1, 2, and 3, respectively.

As documented in Fig. 3A, the increase of the canting angle of the triangular spin structure has only a minor influence on the elastic properties. With increasing field after a small initial increase in fields up to 0.3 T, the sound velocity weakly decreases up to the magnetic phase transition at 11 T, where it exhibits a small kink-like drop (anomaly 1). In clear contrast, the phase between the critical fields of 11 and 25 T is characterized by a tremendous softening of the longitudinal acoustic mode. In this field regime, the manganese spin structure strongly influences the lattice, and exactly at the transition to the plateau regime, the ultrasound velocity exhibits an impressive magnetostructural anomaly, that is, a giant step-like increase by 6% (anomaly 2), indicating an abrupt first-order–like hardening of the elastic constant. Between 25 and 50 T, the longitudinal ultrasound also exhibits a robust plateau, which is terminated by a step-like softening (anomaly 3). Above 50 T, $\Delta v/v$ evidences further continuous softening of the elastic mode up to the highest fields applied in these experiments. These measurements quite impressively document the strong correlation of structural instabilities with spin patterns of the manganese spins and that the magnetization plateau in $MnCr_2S_4$ is stabilized by structural distortions. Figure 3B presents high-field magnetization data at enhanced temperatures between 7.2 and 28 K. Whereas the critical magnetic field of anomaly 1, characterizing the transition from the YK spin structure into an intermediate phase, remains unchanged, the transitions at the critical fields of anomalies 2 and 3 are strongly shifted (indicated by dotted lines in Fig. 3B). At increasing temperatures, all three anomalies are broadened, and at 28 K, the magnetization reveals an almost continuous increase and closely resembles paramagnetic behavior.

Figure 4A presents the relative change of the sound velocity $\Delta v/v$, and Fig. 4B shows the ultrasound attenuation $\Delta\alpha$ as a function of the magnetic field applied along the <111> direction for different temperatures between 1.5 and 16.5 K. The behavior of $\Delta v/v$ observed at 1.5 K was already discussed above. Here, we want to add that a closer inspection of the structural plateau reveals a shallow minimum close to 40 T, indicating a further magnetostructural anomaly (anomaly 4), which has no correspondence in the magnetization results. At temperatures $T > 5$ K, above the YK transition, an additional feature in $\Delta v/v$ appears at low fields (anomaly 5). This anomaly exhibits pronounced hysteresis in pulsed-field experiments. In contrast, static measurements do not show any hysteresis, and the anomalies are significantly shifted to lower fields. These discrepancies between measurements in static and pulsed fields probably result from magnetocaloric effects (*41*). At increasing temperatures, anomaly 5 shifts toward higher fields and finally merges with anomaly 1. Note that as a function of temperature, the critical field of anomaly 1 remains constant, whereas all other anomalies undergo significant shifts. At 11 K, anomaly 2, with a step-like character at lower temperatures, is broadened over a field range from 18 to 25 T, with a clear change of slope at 22 T. Anomaly 4 becomes more pronounced and broadens with increasing temperatures, as indicated by dotted lines in Fig. 4A. At $T > 20$ K, all anomalies become diffuse and lose the characteristics of well-defined phase transitions.

Correspondingly, the ultrasound attenuation exhibits significant features at all magnetostructural transitions (Fig. 4B). These anomalies are only weakly developed at 1.5 K but become dominant at $T > 5$ K. The evolution of damping is highly unusual and exhibits sizable strength at the transitions to the structural plateau: The two peak-like maxima close to 20 and 50 T, which terminate the magnetic and structural plateaus, certainly correspond to critical damping at the magnetostructural phase transitions. At 1.5 and 6 K, when these transitions yield a step-like increase or decrease in the sound velocity, the damping exhibits narrow peak-like maxima. At higher temperatures, when these transitions become more diffusive, the maximum damping shifts toward lower and respectively higher fields.

In the plateau region, specifically at enhanced temperatures $T > 6.2$ K, the damping smoothly decreases from the strongly enhanced low-field and high-field edges toward higher and lower fields, respectively, forming a saddle-like shape. However, at around 40 T, a strong gap-like suppression of damping sets in, resulting in very low, almost temperature-independent values. In this field range, longitudinal sound waves propagate through the crystal with minimum dissipation. In Fig. 4B, this is documented at 6.2, 11, and 16.5 K. At $T = 8.8$ K, this characteristic damping behavior, with

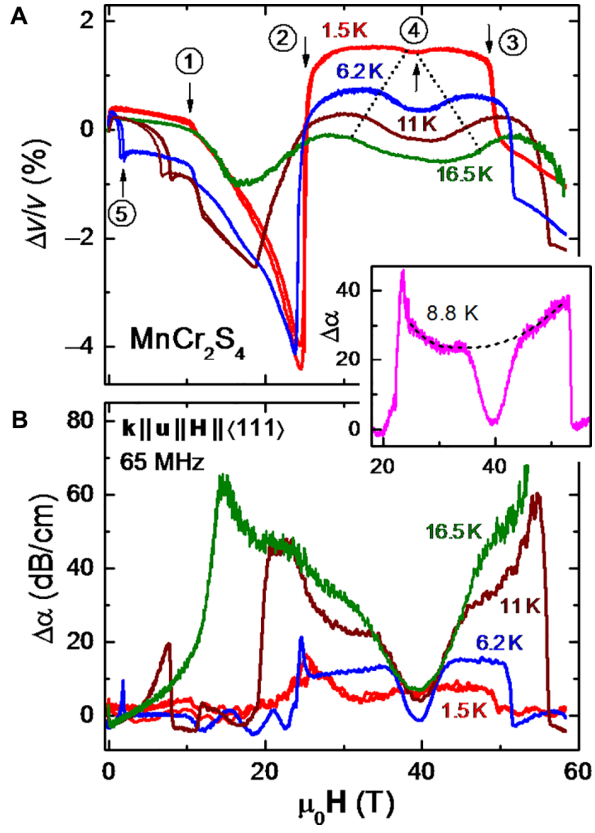

Fig. 4. Field dependence of ultrasound velocity and attenuation in single-crystalline $MnCr_2S_4$. (**A**) Relative change of the sound velocity $\Delta v/v$ of the longitudinal acoustic mode propagating along the <111> axis versus the magnetic field at different temperatures. The external magnetic field was applied parallel to the direction of sound propagation **k** and sound polarization **u**. Arrows mark critical fields at the magnetostructural phase transitions. Dotted lines indicate the broadening of the phase boundaries of anomaly 4. (**B**) Change of the sound attenuation $\Delta\alpha$ versus the magnetic field at different temperatures. The inset highlights the unusual damping behavior at 8.8 K and documents the suppression of damping close to 40 T. This field corresponds to an effective zero magnetic field at the manganese site. The dashed line in the inset is drawn to guide the eye.

a gap-like suppression close to 40 T, is emphasized in the inset of Fig. 4. At this critical field, the AFM Cr–Mn exchange is fully compensated by the external magnetic field, and the *A*-site manganese ions reside effectively in zero field. Here, the spin structure of the manganese moments is only determined by the Mn–Mn exchange, which is strongly bond-frustrated (*2*, *3*). Starting from this dissipationless regime, the damping increases almost exponentially toward smaller ($\mu_0\mathbf{H}$ < 40 T) and larger external fields ($\mu_0\mathbf{H}$ > 40 T). This narrow field range with effectively zero field, where longitudinal sound can propagate almost without dissipation, may host complex spin structures (*42*) or spin liquids (*3*), characteristic of *A*-site spinels, which are, however, invisible for sound propagation.

DISCUSSION

To elucidate the phase diagram, Fig. 5A shows a color-coded plot of the derivative of the sound velocity. Here, we included the critical fields as determined from the field scans of the ultrasound velocity (Fig. 4A) and from magnetization measurements shown in Fig. 3B. We plotted continuous phase boundaries by combining the points of the steepest gradients of the sound velocity but also took the detected anomalies in magnetization (Fig. 3) and damping (Fig. 4B) into account. This results in a highly nontrivial **H**-*T* phase diagram, as discussed in the following.

In zero external magnetic fields and below the ferrimagnetic transition, the chromium moments are aligned in the external field. However, the longitudinal components of the manganese spins are coupled antiferromagnetically with the transverse components still disordered. At low temperatures (*T* < 5 K) and low fields ($\mu_0\mathbf{H}$ < 11.5 T), the triangular YK spin structure is the generally accepted spin configuration (*27*, *37*) and is followed by a metamagnetic transition at 11 T with a significantly steeper increase of the magnetization, indicating a new spin configuration. The existence of a canted triangular structure was proposed early by Plumier (*37*, *38*). However, the absence of any substantial magnetic anisotropy corroborates that the chromium moments always remain parallel to the external field and that only the canted manganese spins rotate with respect to the field direction. The increasing slope in magnetization at higher fields can be understood, assuming that one Mn sublattice points partly in the direction of the external field, resulting in a spin structure as indicated in the phase diagram (Fig. 4A). In this configuration, the longitudinal and the transverse manganese spin components show AFM order, with the net manganese moments still aligned antiparallel to the chromium spins. In the plateau region from 25 to 50 T, the chromium moments are fully field-polarized and ferromagnetically aligned, without any net contributions of the manganese spins to the longitudinal component of the magnetization. In this regime, the manganese moments establish ideal AFM order without any canting within the Mn sublattice. Note that the only possible way to transform the YK spin structure without any jump in the magnetization (as experimentally observed) to the structure with strictly AFM Mn configuration in the plateau regime (where spins are parallel to the field) is to assume the gradual rotation of one of the Mn sublattices with respect to the field.

Concerning the magnetization plateau, we have to mention that at elevated temperature, a slight linear increase of the magnetization is

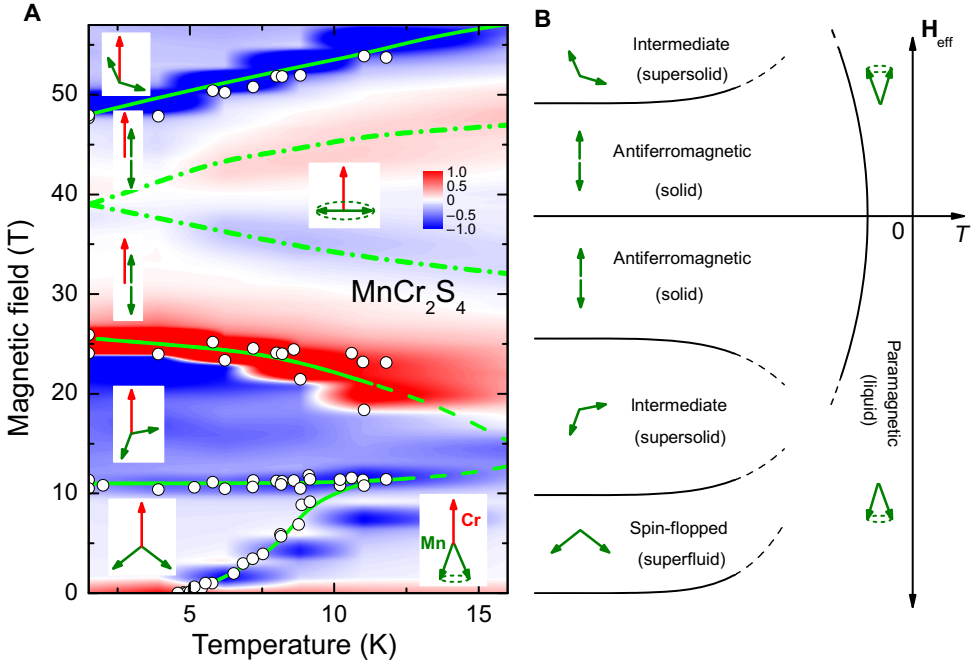

Fig. 5. Thermodynamic phase diagram. (**A**) Color-coded plot of the derivative of the sound velocity *dv*/*d***H.** Open circles represent anomalies in the field-dependent magnetization. The solid lines denote maxima in the field derivatives of the sound velocity, taking the experimentally determined critical fields into consideration. The most probable spin configurations are shown for the different magnetic phases. (**B**) Theoretical phase diagram of a quantum lattice-gas model by Liu and Fisher (*26*). Liquid, superfluid, supersolid, and solid phases are assigned in analogy to bosonic systems, only taking symmetry considerations into account. Only the corresponding spin configurations of the manganese spins are indicated. The chromium moments always follow the external magnetic field and allow for field tuning at the manganese sites from about −40 T < $\mathbf{H}_{eff}$ < 20 T.

observed (shown in Fig. 3 at $T > 5$ K). This increase in magnetization results from thermal excitations of magnons. At the lowest temperature, this slope is significantly reduced because of the freezing out of AFM magnons. This proves the exact collinear alignment of the Mn spins parallel to the external field; otherwise, the slope of the magnetization would be nonzero, independent of temperature due to canting of the Mn sublattices.

Close to 40 T, an unusual phase regime shows up. Its boundaries are indicated by a softening of the acoustic mode at around 40 T (dotted lines in Fig. 4A) and accompanied by a marked gap-like suppression of the ultrasound damping, as shown in the inset of Fig. 4. This regime does not show up in the magnetization (Fig. 3). Hence, we conclude that the manganese spin structure must still be AFM. However, which spin pattern allows for dissipationless propagation of longitudinal sound? Obviously, at 40 T, the sound wave propagation is undisturbed by the manganese spin system. As we have documented in the previous section, the manganese subsystem couples via Cr–Mn exchange striction to sound velocity and damping. At 40 T, the external field exactly compensates the Cr–Mn exchange field, and the manganese spins are completely decoupled from the Cr spins. We conclude that the ideal AFM spin structure of the manganese moments remains unchanged throughout the plateau region but that in the region of decoupled subsystems, manganese spins become ineffective in the damping of ultrasound: The Mn–Cr exchange interaction is completely compensated by the external field, and any two-ion magnetoelastic coupling is effectively zero. At increasing temperatures, this dissipationless regime broadens because thermal excitations additionally compete with the exchange field. At further increasing fields, beyond the plateau regime, an inverted spin structure appears, now with the net moment ferromagnetically aligned parallel to the chromium moments. This sequence of spin structures is shown in Fig. 5A.

In first respect, it is important to note that in the complete **H**-T phase diagram of Fig. 5A, the chromium spins reveal ferromagnetic order and are aligned in an external field beyond 0.3 T. Hence, the field dependences of the magnetization, sound velocity, and sound damping are determined only by the manganese spin texture. Note that the latter two quantities couple to the manganese-spin system via Mn–Cr exchange striction. The phase diagram can be interpreted as that of a pure A-site spinel in external fields between −40 and 20 T. We propose to assign the sequence of manganese spin structures in $MnCr_2S_4$ in analogy to quantum spin systems, where a general relationship with the bosonic lattice-gas model has been established (*25*, *26*). We are aware of the fact that the spin Hamiltonian of $MnCr_2S_4$ discussed so far in literature does not contain anisotropic terms, which at first sight should be essential to work out the analogy. However, besides the isotropic Mn–Mn, Mn–Cr, and Cr–Cr Heisenberg exchange terms, the Hamiltonian contains the biquadratic exchange, which indicates the importance of the spin-lattice coupling (*37*). Penc *et al.* (*12*) have shown that in frustrated magnets, the combination of external magnetic field and spin-lattice coupling provides an alternative route to supersolid phases, even in the absence of magnetic anisotropy. Our results indicate that this can be just the case in $MnCr_2S_4$, where we have strong competition of the AFM and ferromagnetic exchange interactions, leading to bond frustration together with strong spin-lattice coupling evidenced by the ultrasound experiments. The marked correspondence of the phase diagram, as shown in Fig. 5A with theoretical predictions (Fig. 5B) (*26*), led us to the hypothesis that extended supersolid phases may occur in external magnetic fields below and above the plateau region. Consequently using this analogy with quantum lattice-gas models, the plateau region with purely AFM manganese order corresponds to the solid phase characterized by DLRO, whereas the YK phase with canted manganese spins represents the superfluid state. In the superliquid phase, the transverse component of the Mn magnetization is antiferromagnetically ordered, corresponding to ODLRO, whereas the longitudinal component is ferromagnetic, which means absence of DLRO.

Using symmetry considerations, the paramagnetic phase and the field-polarized ferromagnetic state resemble the liquid state without any kind of DLRO or ODLRO. Theoretically, supersolid phases with simultaneous realization of DLRO and ODLRO are expected at the phase boundaries to the crystalline state, that is, in the vicinity of a magnetization plateau because direct continuous transitions between the crystalline and the superliquid phase are forbidden by symmetry. These intermediate phases seem to occur in $MnCr_2S_4$ at the boundaries to the magnetization plateau. The intermediate states manifest extended spin-flop–like regimes, where the canted Mn sublattices gradually approach the collinear AFM state. In our picture, following the study by Penc *et al.* (*12*), this fact results from the combination of strong spin-lattice coupling and an external magnetic field acting on the frustrated Mn spins. This is further evidenced by the observed strong change of the sound velocity, demonstrating the involvement of the lattice and significant spin-lattice coupling, which is important to stabilize the supersolid phase. The strong spin-lattice coupling should also be responsible for the ultra-robust magnetization plateau.

CONCLUSION

To summarize, our high–magnetic field magnetization and ultrasonic experiments on $MnCr_2S_4$ reveal a complex phase diagram and a plethora of fascinating phases. This phase diagram results from the fact that the manganese spins are subject to competing external and exchange fields, and hence, the manganese spins can be tuned between −40 and 20 T. We found an unusual robust magnetization plateau, which is characterized by complete field polarization of the chromium moments and no contributions from the manganese spins. We argue that the AFM order of the manganese subsystem is established throughout the plateau region. However, close to 40 T, where the external field exactly compensates the exchange field, the manganese spins decouple from the Cr sublattice, allowing for sound propagation almost without dissipation.

With this work, we think that we can also contribute to the long-standing debate about supersolidity. Although the question of Leggett (*19*)—"Can a solid be 'superfluid'?"—has not been answered experimentally for solids, our results indicate a possible existence of supersolidity in a spin system. The comparison of the phase diagram with respect to the manganese spins (Fig. 5A) with theoretical predictions (Fig. 5B) suggests the existence of extended supersolid phases, in addition to superfluid and crystalline phases. This direct comparison with theory is possible because we can tune the effective field at the manganese site from plus to minus values. The appearance of an additional phase close to 40 T (that is, effective zero field) results from the complexity of A-site spinels in moderate fields. Together with the recent findings of a low-field spiral spin liquid and a vortex-like spin pattern in the A-site manganese spinel $MnSc_2S_4$ (*9*), our present study of high-field tuned exotic phases in $MnCr_2S_4$ offers a versatile ground for realizing novel properties in frustrated magnets.

MATERIALS AND METHODS

High-quality $MnCr_2S_4$ single crystals were grown by chemical transport reactions. Structure [normal cubic spinel, $Fd3m$, a_0 =1.0117(2) nm] and phase purity were checked by x-ray diffraction technique. Magnetic characterization was performed using a superconducting quantum interference device magnetometer (Quantum Design MPMS 5) at temperatures from 1.8 to 400 K and external magnetic fields up to 5 T. The results are fully compatible with those published in the study by Tsurkan *et al.* (*28*). The high-field magnetization was investigated in pulsed magnetic fields up to 60 T using a compensated pick-up coil system (*43*). The elastic properties were studied by measurements of the sound velocity and attenuation of longitudinal waves, with wave vector **k** and polarization **u** parallel to the <111> axis. This longitudinal mode is related to the elastic constant $c_L = {}^1/_3(c_{11} + 2c_{12} + 4c_{44})$, which is proportional to the square of the sound velocity, assuming cubic crystal symmetry at all temperatures and fields. These measurements were performed in static magnetic fields up to 17 T at temperatures between 1.5 and 300 K and in pulsed magnetic fields up to 60 T from 1.5 to 75 K. The pulsed-field measurements used magnetic field pulses with a duration of 150 ms and with a rise time of 35 ms. A standard pulse-echo method (*44*) with phase-sensitive detection technique was used in all ultrasound measurements.

REFERENCES AND NOTES

1. P. W. Anderson, Ordering and antiferromagnetism in ferrites. *Phys. Rev.* **102**, 1008–1013 (1956).
2. L. Balents, Spin liquids in frustrated magnets. *Nature* **464**, 199–208 (2010).
3. D. Bergman, J. Alicea, E. Gull, S. Trebst, L. Balents, Order-by-disorder and spiral spin-liquid in frustrated diamond-lattice antiferromagnets. *Nat. Phys.* **3**, 487–491 (2007).
4. G. Chen, L. Balents, A. P. Schnyder, Spin-orbital singlet and quantum critical point on the diamond lattice: $FeSc_2S_4$. *Phys. Rev. Lett.* **102**, 096406 (2009).
5. V. Fritsch, J. Hemberger, N. Büttgen, E.-V. Scheidt, H.-A. K. von Nidda, A. Loidl, V. Tsurkan, Spin and orbital frustration in $MnSc_2S_4$ and $FeSc_2S_4$. *Phys. Rev. Lett.* **92**, 116401 (2004).
6. A. Krimmel, M. Müksch, V. Tsurkan, M. M. Koza, H. Mutka, A. Loidl, Vibronic and magnetic excitations in the spin-orbital liquid state of $FeSc_2S_4$. *Phys. Rev. Lett.* **94**, 237402 (2005).
7. L. Mittelstädt, M. Schmidt, Z. Wang, F. Mayr, V. Tsurkan, P. Lunkenheimer, D. Ish, L. Balents, J. Deisenhofer, A. Loidl, Spin-orbiton and quantum criticality in $FeSc_2S_4$. *Phys. Rev. B* **91**, 125112 (2015).
8. N. J. Laurita, J. Deisenhofer, L.-D. Pan, C. M. Morris, M. Schmidt, M. Johnsson, V. Tsurkan, A. Loidl, N. P. Armitage, Singlet-triplet excitations and long-range entanglement in the spin-orbital liquid candidate $FeSc_2S_4$. *Phys. Rev. Lett.* **114**, 207201 (2015).
9. S. Gao, O. Zaharko, V. Tsurkan, Y. Su, J. S. White, G. S. Tucker, B. Roessli, F. Bourdarot, R. Sibille, D. Chernyshov, T. Fennell, A. Loidl, C. Rüegg, Spiral spin-liquid and the emergence of a vortex-like state in $MnSc_2S_4$. *Nat. Phys.* **13**, 157–167 (2016).
10. H. Ueda, H. A. Katori, H. Mitamura, T. Goto, H. Takagi, Magnetic-field induced transition to the 1/2 magnetization plateau state in the geometrically frustrated magnet $CdCr_2O_4$. *Phys. Rev. Lett.* **94**, 047202 (2005).
11. A. Miyata, H. Ueda, Y. Ueda, H. Sawabe, S. Takeyama, Magnetic phases of a highly frustrated magnet, $ZnCr_2O_4$, up to an ultrahigh magnetic field of 600 T. *Phys. Rev. Lett.* **107**, 207203 (2011).
12. K. Penc, N. Shannon, H. Shiba, Half-magnetization plateau stabilized by structural distortion in the antiferromagnetic Heisenberg model on a pyrochlore lattice. *Phys. Rev. Lett.* **93**, 197203 (2004).
13. M. Matsuda, H. Ueda, A. Kikkawa, Y. Tanaka, K. Katsumata, Y. Narumi, T. Inami, Y. Ueda, S.-H. Lee, Spin–lattice instability to a fractional magnetization state in the spinel $HgCr_2O_4$. *Nat. Phys.* **3**, 397–400 (2007).
14. V. Tsurkan, S. Zherlitsyn, V. Felea, S. Yasin, Y. Skourski, J. Deisenhofer, H.-A. K. von Nidda, P. Lemmens, J. Wosnitza, A. Loidl, Magnetostructural transitions in a frustrated magnet at high fields. *Phys. Rev. Lett.* **106**, 247202 (2011).
15. V. Felea, S. Yasin, A. Günther, J. Deisenhofer, H.-A. K. von Nidda, S. Zherlitsyn, V. Tsurkan, P. Lemmens, J. Wosnitza, A. Loidl, Spin–lattice coupling in the frustrated antiferromagnet $ZnCr_2Se_4$ probed by ultrasound. *Phys. Rev. B* **86**, 104402 (2012).
16. T. Rudolf, C. Kant, F. Mayr, J. Hemberger, V. Tsurkan, A. Loidl, Spin-phonon coupling in antiferromagnetic chromium spinels. *New J. Phys.* **9**, 76 (2007).
17. V. Tsurkan, S. Zherlitsyn, S. Yasin, V. Felea, Y. Skourski, J. Deisenhofer, H.-A. K. von Nidda, J. Wosnitza, A. Loidl, Unconventional magnetostructural transition in $CoCr_2O_4$ at high magnetic fields. *Phys. Rev. Lett.* **110**, 115502 (2013).
18. T. Giamarchi, C. Rüegg, O. Tchernyshyov, Bose–Einstein condensation in magnetic insulators. *Nat. Phys.* **4**, 198–204 (2008).
19. A. J. Leggett, Can a solid be "superfluid"? *Phys. Rev. Lett.* **25**, 1543–1546 (1970).
20. E. Kim, M. H. W. Chan, Probable observation of a supersolid helium phase. *Nature* **427**, 225–227 (2004).
21. D. Y. Kim, M. H. W. Chan, Absence of supersolidity in solid helium in porous Vycor glass. *Phys. Rev. Lett.* **109**, 155301 (2012).
22. A. Miyata, H. Ueda, Y. Ueda, H. Sawabe, S. Takeyama, Magnetic phases of $ZnCr_2O_4$ revealed by magneto-optical studies under ultra-high magnetic fields of up to 600 T. *J. Phys. Soc. Jpn.* **81**, 114701 (2012).
23. A. Miyata, S. Takeyama, H. Ueda, Magnetic superfluid state in the frustrated spinel oxide $CdCr_2O_4$ revealed by ultrahigh magnetic fields. *Phys. Rev. B* **87**, 214424 (2013).
24. A. Miyata, H. Ueda, S. Takeyama, Canted 2:1:1 magnetic supersolid phase in a frustrated magnet $MgCr_2O_4$ as a small limit of the biquadratic spin interaction. *J. Phys. Soc. Jpn.* **83**, 063702 (2014).
25. H. Matsuda, T. Tsuneto, Off-diagonal long-range order in solids. *Prog. Theor. Phys. Suppl.* **46**, 411–436 (1970).
26. K.-S. Liu, M. E. Fisher, Quantum lattice gas and the existence of a supersolid. *J. Low Temp. Phys.* **10**, 655–683 (1973).
27. F. K. Lotgering, Spin canting in $MnCr_2S_4$. *J. Phys. Chem. Solids* **29**, 2193–2197 (1968).
28. V. Tsurkan, M. Mücksch, V. Fritsch, J. Hemberger, M. Klem, S. Klimm, S. Körner, H.-A. K. von Nidda, D. Samusi, E.-V. Scheidt, A. Loidl, S. Horn, R. Tidecks, Magnetic, heat capacity, and conductivity studies of ferrimagnetic $MnCr_2S_4$ single crystals. *Phys. Rev. B* **68**, 134433 (2003).
29. T. A. Kaplan, Classical theory of spin configurations in the cubic spinel. *Phys. Rev.* **119**, 1460–1470 (1960).
30. D. H. Lyons, T. A. Kaplan, K. Dwight, N. Menyuk, Classical theory of the ground spin-state in cubic spinels. *Phys. Rev.* **126**, 540–555 (1962).
31. N. Menyuk, K. Dwight, A. Wold, Magnetic properties of $MnCr_2S_4$. *J. Appl. Phys.* **36**, 1088–1089 (1965).
32. R. Plumier, M. Sougi, Étude par diffraction des neutrons d'une transition magnétique á basse température dans le thiospinele $MnCr_2S_4$. *C. R. Acad. Sci.* **268**, 1549–1552 (1969).
33. M. Nauciel-Bloch, A. Castets, R. Plumier, Sublattice magnetizations and magnetostrictive effects in sulphospinel $MnCr_2S_4$. *Phys. Lett.* **39**, 311–312 (1972).
34. R. Plumier, M. Sougi, Neutron diffraction reinvestigation of $MnCr_2S_4$. *Mater. Sci. Forum* **133–136**, 523–528 (1993).
35. Y. Yafet, C. Kittel, Antiferromagnetic arrangements in ferrites. *Phys. Rev.* **87**, 290–294 (1952).
36. J.-M. Denis, Y. Allain, R. Plumier, Magnetic behavior of $MnCr_2S_4$ in high magnetic fields. *J. Appl. Phys.* **41**, 1091–1093 (1970).
37. R. Plumier, Étude de l'influence du terme d'échange biquadratique sur les comportement d'un spinelle ferrimagnétique normal en presénce d'un champ magnétique intense. *C. R. Acad. Sci.* **271**, 184 (1970).
38. R. Plumier, The magnetic structure of sulfur spinel $MnCr_2S_4$ under applied magnetic field. *J. Phys. Chem. Solids* **41**, 871–873 (1980).
39. L. Goldstein, P. Gibart, M. Mejai, M. Perrin, Magnetic structures of the spinels compounds $MnCr_{2-x}V_xS_4$. *Physica B* **86–88**, 893–895 (1977).
40. M. Nogues, M. Mejaï, L. Goldstein, Phase relationships and magnetic phase diagram in the system $Mn_{1-x}Cu_xCr_2S_4$. *J. Phys. Chem. Solids* **40**, 375–379 (1979).
41. V. Zapf, M. Jaime, C. D. Batista, Bose-Einstein condensation in quantum magnets. *Rev. Mod. Phys.* **86**, 563–614 (2014).
42. A. Krimmel, M. Mücksch, V. Tsurkan, M. M. Koza, H. Mutka, C. Ritter, D. V. Sheptyakov, S. Horn, A. Loidl, Magnetic ordering and spin excitations in the frustrated magnet $MnSc_2S_4$. *Phys. Rev. B* **73**, 014413 (2006).
43. Y. Skourski, M. D. Kuz'min, K. P. Skokov, A. V. Andreev, J. Wosnitza, High-field magnetization of Ho_2Fe_{17}. *Phys. Rev. B* **83**, 214420 (2011).
44. S. Zherlitsyn, S. Yasin, J. Wosnitza, A. A. Zvyagin, A. V. Andreev, V. Tsurkan, Spin–lattice effects in selected antiferromagnetic materials. *Low Temp. Phys.* **40**, 160–172 (2014).

Acknowledgments: We thank P. Lunkenheimer for help in preparing the figures and for useful discussions. **Funding:** This research was supported by the German Research Foundation (DFG) through the Transregional Collaborative Research Center TRR 80 (Augsburg, Munich, and Stuttgart) and the Collaborative Research Center (SFB) 1143 (Dresden). We acknowledge support of Hochfeld-Magnetlabor Dresden (HLD) at the Helmholtz-Zentrum Dresden-Rossendorf, a member of the European Magnetic Field Laboratory. **Author contributions:** V.T., Z.W., J.D., H.-A.K.v.N., and A.L. performed susceptibility and magnetization characterizations of the samples in static magnetic fields, evaluated the data, constructed the phase diagram, and interpreted the results. V.T. and L.P. prepared the single crystals. S.Z., P.T.C., V.F., Y.S., and J.W. performed ultrasound and magnetization measurements in static and pulsed fields. A.L., V.T., and H.-A.K.v.N. prepared the manuscript with input from all coauthors. All authors contributed extensively to this work. **Competing interests:** The authors declare that they have no competing interests.

Data and materials availability: All data needed to evaluate the conclusions in the paper are present in the paper. Additional data related to this paper may be requested from the authors.

Submitted 22 August 2016
Accepted 31 January 2017
Published 17 March 2017
10.1126/sciadv.1601982

Citation: V. Tsurkan, S. Zherlitsyn, L. Prodan, V. Felea, P. T. Cong, Y. Skourski, Z. Wang, J. Deisenhofer, H.-A. K. von Nidda, J. Wosnitza, A. Loidl, Ultra-robust high-field magnetization plateau and supersolidity in bond-frustrated $MnCr_2S_4$. *Sci. Adv.* **3**, e1601982 (2017).

Science Advances

Ultra-robust high-field magnetization plateau and supersolidity in bond-frustrated $MnCr_2S_4$

Vladimir Tsurkan, Sergei Zherlitsyn, Lilian Prodan, Viorel Felea, Pham Thanh Cong, Yurii Skourski, Zhe Wang, Joachim Deisenhofer, Hans-Albrecht Krug von Nidda, Joahim Wosnitza and Alois Loidl

Sci Adv **3** (3), e1601982.
DOI: 10.1126/sciadv.1601982